Possibility of the Magnetic Field Effect on the Thermal Decomposition N_2O: Molecular Dynamics Simulation.

Osamu TAKAHASHI, Naotake KURUSHIMA, Akio KAWANO,
and Ko SAITO*
Department of Chemistry, Graduate School of Science, Hiroshima University,
1-3-1, Kagamiyama, Higashi-Hiroshima 739-8526, JPN

Abstract

Molecular dynamics model calculations for the thermal decomposition of N_2O with external magnetic field were performed. The effect of external magnetic field was modeled by parameterization of the interaction term between the singlet and triplet potential surfaces. It was suggested that the increase of the rate constant by external magnetic field could be explained by means of the increase of interaction term which is dependent on the angle of the Jacobi coordinate.

1 Introduction

Until the early 1970's, most scientists believed that the magnetic field could not exert appreciable effects upon chemical reactions because of its much smaller energy compared with the ordinary activation energy of chemical reactions. However, it has been admitted that an ordinary magnetic field affects the predissociation of iodine vapor and the interconversion of *ortho-* and *para-* hydrogen [1]. One of the interesting scientific problems is to control chemical and biological reactions with external magnetic fields [2]. At the 1970's magnetic quenching was found for fluorescence from an excited singlet state of CS_2 in the gas phase [3, 4] and in the dissociation reaction system including biradicals [2, 5, 6]. Then the magnetic effects have been studied for many reaction systems from both experimental and theoretical point of view.

Recently, Saito et al. [7] observed that the external magnetic field of about 2 kG at temperatures higher than 2000K accelerated the following reaction,

$$N_2O \longrightarrow N_2(^1\Sigma_g^+) + O(^3P). \tag{1}$$

Both the rate constant and activation energy were higher than that for the reaction without magnetic field. Schematic potential energy diagram of the N_2O molecule is shown in Fig. 1. In the analysis of this reaction, non-adiabatic transition between the singlet and triplet surfaces is included. Saito et al. [7] suggested that the crossing point at which strong interaction occurs between the potential surfaces was changed by the external magnetic field, and that the transition became easier at some crossing point which was higher energy level than the usual transition point with no magnetic field.

Some theoretical studies have been performed to investigate the potential energy surface(PES) in a strong magnetic field [8, 9] and dynamics on the PES [10]. According to these studies, the effect on the dissociation rate by the weak magnetic field such as 2 kG is estimated to be negligibly small. Theoretical investigations on the PES of N_2O were performed including the spin-forbidden process in the de-

composition [11, 12]. Chang et al. [13] re-estimated the empirical potential energy surface proposed by Zahr et al [11]. Recently, Nakamura and Kato [14] estimated a very accurate potential energy surface by *ab initio* molecular orbital calculations.

Marks and Thompson [15, 16] performed molecular dynamics(MD) calculations for the N_2O dissociation process. They theoretically estimated the dissociation rate of N_2O and concluded that this reaction is mode-specific spin-forbidden reaction. Chang and Yarkony [13] proposed a new dissociation path via the 2^3A" state which was higher state than the 1^3A" state. According to their paper, the spin-orbit interaction between 1^1A'(the ground state of N_2O) and the 2^3A" state is a few cm^{-1}, that is, even if the reaction is affected by the external magnetic field, it seemed difficult to explain the experimental results reported in Ref. [7].

In previous studies treated dinamically by Zahr et al. [11] and Marks and Thompson [15,16], the spin-orbit interaction of N_2O, which included a non-adiabatic interaction term, was treated to be constant. On the other hand, Chang and Yarkony [13] and Nakamura and Kato [14] treated this interaction as a variable depending on the molecular configuration, taking a maximum when N-N-O is collinear. To examine the magnetic field effect on the decomposition rate of N_2O, we extended the interaction term between the singlet and triplet surfaces as a function of the angle N-N-O. Also, MD simulations were performed to examine the influence of the interaction term.

2 Theory

Total Hamiltonian with external magnetic field is postulated as follows [17],

$$H = H_0 + H_{SO} + H_{mag} + H_Z \tag{2}$$

where H_0 is the term without the relativistic interaction and external magnetic field, H_{SO} is the spin-orbit interaction, H_{mag} is the external magnetic fields interacting with electronic orbital motion, and H_Z is the interaction between electron spin and

magnetic field. H_{SO} in Eq. (2) is expressed as follows,

$$H_{SO} = \frac{g\beta^2}{4\pi\varepsilon_0 c^2}[\sum_{n,i} \frac{Z_n \mathbf{S}(i) \cdot \mathbf{L}_n(i)}{r_{ni}^3} - \sum_{i,j}{}' \frac{2\mathbf{S}(i) \cdot \mathbf{L}_i(j) + \mathbf{S}(i) \cdot \mathbf{L}_j(i)}{r_{ij}^3}] \tag{3}$$

where, $S(i)$ is the spin angular momentum operator of electron i, $L_i(j)$ is the angular momentum operator of the jth atom, Z_n is the charge of the nth atom. The influence of the external magnetic field for nuclei is negligibly small. Interaction term between nuclears is also very small compared with that between electrons, that is, H_{SO} is nearly constant. H_{mag} in Eq. (2) is expressed by two terms, these are the first and second order term for the external magnetic field [17],

$$H_{mag} = \beta \sum_i \mathbf{B} \cdot \mathbf{L}(i) + \frac{e^2}{8m} \sum_i (\mathbf{B} \times \mathbf{r}_i)^2, \tag{4}$$

where $\mathbf{B}$ is the uniform external magnetic field, $\mathbf{L}(i)$ is the angular momentum operator of the ith atom, and β is the Bohr magneton. The first term in Eq. (4) gives the orbital paramagnetism of free atoms in states with non-zero angular momentum. But in second order it also contributes to diamagnetism, reducing the main contribution which arises from the second term. Eq. (4) means that the anisotropy of the orbital varies with the change of the electron motion by the external magnetic field. H_Z is simply the electron spin-field coupling given by

$$H_Z = g\beta \sum_i \mathbf{B} \cdot \mathbf{S}(i) \tag{5}$$

and gives the orbitally independent part of the Zeeman effect. The orbital contribution, sometimes included in a Zeeman term of the form $\beta \sum_i \mathbf{B} \cdot [\mathbf{L}(i) + g\mathbf{S}(i)]$, arises in fact from the first term of Eq. (4), which is dealt separately.

Next, the total wavefunction of system will be supposed to the next equation,

$$|\Phi >= |\Psi_1 > + |\Psi_2 >, \tag{6}$$

where $|\Psi_1 >$ and $|\Psi_2 >$ are the singlet and triplet wavefunctions, respectively. Furthermore, it will be assumed that each state is only one in each multiplicity. Thus, the following time-independent Schrödinger equation can be solved,

$$H|\Phi >= E|\Phi > . \tag{7}$$

The diagonal elements of Eq. (7) are potential energy for the singlet and triplet surfaces. And the off-diagonal element is the interaction term between two states,

$$V_i =< \Psi_i|H|\Psi_i > \tag{8}$$

for i = 1 and 2, and

$$V_{12} =< \Psi_1|H|\Psi_2 > . \tag{9}$$

As stated above, there is an interaction of atomic motion with magnetic field, which means that the Hamiltonian for molecule with external magnetic field include the angular momentum operators, i.e., the interaction is anisotropic.

In the model of gas phase reaction, the MD simulation seems to be a powerful tool. However, as a practical problem, it is difficult to apply it to the effect of atomic motion with the external magnetic field explicitly. Thus, we tried to simplify this effect to perform the MD calculations as in the following sections.

3 Methods of Calculation

We investigate the N_2O thermal decomposition process using MD calculations. On this paper, we describe our procedure in detail.

3.1 Potential energy surfaces

In the previous papers [11, 13, 14], potential surfaces of the N_2O molecule were proposed both for the singlet and triplet states. The potential energy surfaces used in this work are those of Zahr et al. [11] presented in their study of the quenching of $O(^1D)$ by N_2, in order to compare our calculated rate constant with those of Marks et al [15,16]. Their potential energy surfaces, both for the singlet and triplet states, are expressed by the Jacobi coordinate, defined by Fig. 2, where r is the $N-N$ bond distance, R is the distance between O atom and the center-of-mass of N_2, and γ is the angle between vector $\mathbf{r}$ and $\mathbf{R}$.

3.2 Decision of transition

Thermal decomposition process of N_2O to $N_2(^1\Sigma_g^+)$ and $O(^3P)$ include non-adiabatic transition process between the singlet and triplet surfaces. The transition between two surfaces is accounted to occur when trajectory of the MD simulation pass the crossing point of the two potential surfaces, in the way whether the sign of the difference between the two potential surfaces change or not,

$$\Delta V(t) = V_1(t) - V_2(t). \tag{10}$$

If the signs of $\Delta V(t)$ and $\Delta V(t - \Delta t)$ are the same, the trajectory does not over the crossing point. On the other hand, if the signs are different, it is found that the trajectory passed the crossing point in the time interval between $t - \Delta t$ and t. The time that trajectory passed through the crossing point is defined as t_c.

The transition probability is calculated when the trajectory passes the crossing point. At each crossing point, we calculate the Landau-Zener transition probability [18] for a single passage through the crossing surfaces,

$$P_{LZ} = 1 - \exp \frac{-2\pi V_{12}^2}{\hbar |\Delta \mathbf{F} \cdot \mathbf{v}|}, \tag{11}$$

where V_{12} is the interaction term which couples the two potential surfaces. The term V_{12} will be discussed later. $\Delta \mathbf{F}$ is the difference in the forces $\mathbf{F_1}$ and $\mathbf{F_2}$ of the lower and upper states, respectively, evaluated at the crossing point, while $\mathbf{v}$ is the nuclear velocity at the crossing point.

To estimate Eq. (11), it is necessary to calculate the coordinate $\{ q_i(t_c) \}$, the momentum $\{ p_i(t_c) \}$, the gradient of the potential surface $\{ \partial V_1/\partial q_i \}$ and $\{ \partial V_2/\partial q_i \}$ at the time of the crossing point. Marks et al. [15] calculated the following scheme: when the sign of $\Delta V(t)$ is changed, the trajectory is propagated along opposite time by a small time step. When the energy difference between the two potential energy surfaces is very small, the quantities can be obtained.

However, if this method is used, trajectory calculation must be propagated along opposite time whenever the trajectory passes the crossing point, and it causes the

increase of the computational time. In order to avoid this problem, we use the interpolation as an appropriate method.

In the case of very small time step, the gradients of both the singlet and triplet potential surfaces near the crossing point are taken to be constant approximately. Then, by using the absolute value of $\Delta V(t)$ instead of the relative value,

$$\mathbf{A}(t_c) = \mathbf{A}(t - \Delta t) + (\mathbf{A}(t) - \mathbf{A}(t - \Delta t))\frac{\Delta V(t - \Delta t)}{\Delta V(t - \Delta t) + \Delta V(t)}, \tag{12}$$

where vector $\mathbf{A}$ represents coordinate $\mathbf{q}$, momentum $\mathbf{p}$, and gradients of the potential V_1 and V_2. The time passed through the crossing point is

$$t_c = t + \Delta t\frac{\Delta V(t - \Delta t)}{\Delta V(t - \Delta t) + \Delta V(t)}. \tag{13}$$

Since this method is not need the time propagation step to the opposite time, we can calculate the crossing point at minimum cost.

When the trajectory is reached the crossing point, the judgment of transition is performed. Transition probability P_{LZ} is compared to uniform random number R [0,1], and if $P_{LZ} > R$, then transition is happened and the propagation of this trajectory is stopped, or the propagation is continued.

3.3 Estimation of magnetic field effect

In our simulation, it is important to estimate the interaction term V_{12} in Eq. (11). According to Zahr et al. [11], V_{12} is equal to the spin-orbit term, and is constant. Marks et al. [15, 16] used their potential surface. Chang et al. [13] performed *ab initio* calculations and concluded that the spin-orbit term is not constant and H_{SO} takes the highest value when N_2O is collinear. Although the main component of V_{12} is the spin-orbit term, other contributions must be considered. To construct a simple model for the transition between the singlet and triplet surfaces, we use the expression for V_{12},

$$V_{12} = A + B\cos 2\gamma, \tag{14}$$

where A and B are constants and γ is Jacobi coordinate for N_2O molecule. Our model is somewhat complicated compared to the previous model for the non-adiabatic transition of N_2O. In the case of without the external magnetic field, we adopt $A = 80$ cm^{-1} and $B = 50$ cm^{-1}. Compared with Chang et al. [13], our parameters overestimate the spin-orbit term for the collinear case, but a merit of this larger parameter is to include another factor for the interaction term effectively. Parameter A is independent of molecular configuration and is a molecular-specific parameter. On the other hand, parameter B is dependent on molecular configuration and corresponds to the anisotropic term. Furthermore, as Eq. (4) shows, the magnetic field term includes the angular momentum operator, thus, we postulate that these parameters vary with the external magnetic field. In comparison to the case without the external magnetic field, the interaction term is perturbed by the external magnetic field. Actual interaction is indeed more complicated, and can not formulate using some simple functions, as shown the last section. Since our objective is to estimate the dissociation rate constant of N_2O, we adopt a simplified Eq. (14) to avoid time-consuming step.

3.4 Trajectory calculation

Trajectory calculations are performed with the total energy range between 65 to 85 kcal mol^{-1}. The sampling of initial geometry and velocity with microcanonical distributions of energy were performed using the "efficient microcanonical sampling"(EMS) method [19, 20] with no rotational angular momentum [21]. For each energy, 5000 trajectories run, and its total trajectory length for each run is 10 ps. A large number of trajectories lowers the fluctuation of the rate constant for each total energy. We use the 6-th symplectic integrator [22] with time step of 0.4 fs. The symplectic integrator is numerical integration schemes for Hamiltonian systems, which conserve the symplectic two-form $dp \wedge dq$ exactly, so that $(q(0), p(0)) \longrightarrow (q(\tau), p(\tau))$ is a canonical transformation. This algorithm is accurate and has no accumulation

of numerical errors for total energy in contrast to the other common algorithm to solve the Hamilton equation of motion. Practically, the elapsed time for each time step wastes compared with common integrator, such as the Runge-Kutta method. However, if accuracy of the same order are requested for the energy conservation, we can set up longer time step. Rate constant $k(E)$ is obtained from least-square fitting of the equation,

$$\ln \frac{N_t}{N_0} = -k(E)t, \tag{15}$$

where N_t is the number of non-reactive trajectories at time t and N_0 is the number of total trajectories.

4 Results and discussion

4.1 Dependence of the rate constant on various conditions

To look for the best condition of trajectory calculations, we first examine the dependence of the rate constant for various conditions. It is considerable that there are some causes which make rate constant vary for conditions of simulation; for example, Markov walk number for the EMS method and propagating time step. In the present work, 1000 trajectories run with the interaction term $V_{12} = 80$ cm^{-1}(constant) for all conditions. Under these conditions, it is expected that the number of reactive trajectories and transition probability are changed and, thus, microcanonical rate constants $k(E)$ are changed.

Markov walk number dependencies for the EMS method are shown in Table 1. Under these conditions, we use the 6-th symplectic integrator with propagating time step of 0.4 fs. Marks et al. [15] generated twenty thousand states. In general, if the number of the Markov walk and trajectories are small, the rate constant depends on the initial geometry. In our simulations, if the available energy is low, the explicit dependency on the Markov walk number becomes clear for small walk number. However, if the available energy is fairly large, the dependency becomes

ambiguous, thus we take a large number of trajectories. In order to treat under the same conditions as Marks et al., we took 10,000 for the number of Markov walk.

Time step dependence for the trajectory calculation are shown in Table 2. As the integrator of equation of motion, both the 4th Runge-Kutta and the 6th symplectic methods are used. When the time step of trajectory calculations using the former method is larger than 0.2 fs, the total energy decreases considerably because of cumulative numerical error, i.e., conservation of total energy is not guaranteed. Although the rate constant should be independent of the integrator and of the time step, it is clearly changed for the long time step as shown in Table 2, suggesting that this approach is not suitable. Furthermore, if the time step is fairly large, the trajectories which graze the crossing curve are not counted.

Distribution of transition point are shown in Figs. 3 and 4. Number of trajectories are 5000 and total energies are 85 kcal mol^{-1}. In these figures, one coordinate(R for Fig. 3 and r for Fig. 4) is fix. In the case of V_{12}=constant, $B = 0$, in Eq. (14), transition points are uniformly distributed. On the other hand, in the case of which the parameter B is not zero, transition points distribute near collinear region, i.e., near $\gamma = 0$. It is caused that we adopt to V_{12} that is the largest in the case of collinear configuration.

4.2 Rate constant k

Results of microcanonical rate constant $k(E)$ are shown in Table 3. When V_{12} is constant, our simulation corresponds to the condition of Marks et al. Our microcanonical rate constants give always a little smaller values than those of them. This may be arisen from the different sampling of the initial condition or using the different potential energy surfaces. However, the tendency is comparable to Marks et al. It means that V_{12} shows an angular dependency ($A = 80$ and $B = 50$ cm^{-1}), i.e., rate constants are a little larger for variable V_{12}. This is based on the fact that using Eq. (14), the interaction term between the singlet and triplet surfaces becomes

larger in the case of collinear configuration compared to the case of V_{12}=constant. The parameters A and B are varied to examine anisotropic dependency for the interaction term V_{12}. On this paper, we compare the rate constants at 2000K, since the experimental temperature range are 1800-2300 K. From a shock tube experiment, Arrhenius expressions for bimolecular reaction rates with and without external magnetic field are given in reference [7]. It is found that the rate constant of N_2O decomposition with 2kG external magnetic field is about 19 % larger than without magnetic field at 2000 K. In order to compare the experimental rate constant, calculated microcanonical rate constant k_{MC} is convert to canonical rate constant k_{CA} multiplied by Boltzmann factor,

$$k_{CA} = \frac{\sum_N k_{MC} \exp(-E/k_B T)}{\sum_N \exp(-E/k_B T)}. \tag{16}$$

Numerical canonical rate constants at 2000 K with experimental rate constant are shown in Table 4. In our simulations, since classical mechanics and empirical potential energy surfaces are used, it is difficult to discuss quantitatively the value of the rate constant. However, we could compare the ratio between rate constants with and without the external magnetic field, and also compare with the ratio obtained from our model calculation.

Our calculated results are shown in Table 5. The ratio is the value divided by the rate constant in the case of $A = 80$ and $B = 50$ cm^{-1}. It is natural that rate constants become large when parameters A and B also become large. As seen in this table, the ratio increases with increasing parameters A and B. This explains qualitatively the experimental results. To give the experimental ratio(19 %), the value should be increased by about 15 cm^{-1} for the parameter A, while it should be increased by about 20 cm^{-1} for the parameter B. The first term of Eq. (14) is independent of the angle and is considered to be a characteristic parameter of molecule, which is not expected to change largely. On the other hand, the second term is dependent on the angle, and therefore, V_{12} could be affected by external magnetic field resulting the change of the rate constant. Hence, we found out that

there is a possibility of the magnetic field effect on the chemical reaction.

5 Summary

To explain the experimental results of enlargement of the dissociation rate constant for N_2O to $N_2(^1\Sigma^+)$ and $O(^3P)$ with external magnetic field, MD simulations were performed. Interaction term between the singlet and triplet surfaces was modeled by two parameters, which one is dependent on the angle of the Jacobi coordinate, and the other is independent on it. According to our rough model, the increase of the rate constant can be explained by increasing of the non-adiabatic interaction term, especially the angle dependent term. In this field, there is no sufficient investigation both in experiment and theory. We will continue further investigations in the future.

6 Acknowledgement

This study is supported by a Grant-in-Aid on Research for the Future "Photoscience" (JSPS-RFTF-98P01202) from Japan Society for the Promotion of Science. The authors thank the Institute for Non-linear Science and Applied Mathematics at Hiroshima University, for the use of COMPAQ Personal Workstation 433au, and the Instrument Center for Chemical Analysis, Hiroshima University, for the use of SGI Indigo2.

References

[1] H. Hayashi, Magnetic field effects on dynamic behavior and chemical reactions of excited molecules, CRC Press,Inc, Boca Raton, Florida, 1990, Ch. 2, p. 59.

[2] S.Wilson (Ed.), Methods in Computational Chemistry, Vol. 2, Plenum, New York, 1988.

[3] A.Matsuzaki, S.Nagakura, Chem. Lett. (1974) 675.

[4] H.Abe, H.Hayashi, Chem. Phys. Lett. 187 (1991) 227.

[5] H.Hayashi, Y.Sakuragi, CRC Press,Inc, Boca Raton, Florida, 1990, p. 1.

[6] U.E.Steiner, T.Ulrich, Chem. Rev. 89 (1989) 51.

[7] K.Saito, Y.Kawaguchi, K.Suzuki, O.Takahashi, K.Tabayashi, Proceedings of the 21th International Symposium on Shock Waves, ISSW21 (1997) 8240.

[8] U.Kappes, P.Schmelcher, Phys. Rev. A 54 (1996) 1313.

[9] K.Kamiya, H.Matsui, Bull. Chem. Soc. Jpn. 64 (1991) 2792.

[10] T.P.Grosdanov, J. Phys. B 18 (1985) 921.

[11] G.E.Zahr, R.K.Preston, W.H.Miller, J. Chem. Phys. 62 (1975) 1127.

[12] G.Yan, H.Xian, D.Xie, Chem. Phys. Lett. 271 (1997) 157.

[13] A.H.H.Chang, D.R.Yarkony, J. Chem. Phys. 99 (1993) 6824.

[14] T.Nakamura, S.Kato, J. Chem. Phys. 110 (1999) 9937.

[15] A.J.Marks, D.L.Thompson, J. Chem. Phys. 95 (1991) 8056.

[16] A.J.Marks, D.L.Thompson, J. Chem. Phys. 96 (1992) 1911.

[17] R.McWeeny, Methods of Molecular Quantum Mechanics, Academic Press, London, 1992.

[18] C.Zener, Proc. R. Soc. London Ser. A 137 (1932) 696.

[19] E.S.Severin, B.C.Freasier, N.D.Hamer, D.L.Jolly, S.Nordholm, Chem. Phys. Letters 57 (1978) 117.

[20] H.W.Schranz, S.Nordholm, G.Nyman, J. Chem. Phys. 94 (1991) 1487.

[21] G.Nyman, S.Nordholm, H.W.Schranz, J. Chem. Phys. 93 (1990) 6767.

[22] H.Yoshida, Phys. Letters A 150 (1990) 262.

Table 1: Rate constant(in ps^{-1}) dependency for Markov walk number. Other trajectory conditions are as followed: integrator is the 6th Symplectic method, time step of propagation is 0.4 fs, and 1000 trial run. Rate constant for 5000 trial run are also shown.

	total energy / kcal mol^{-1}				
number of Markov walk	65	70	75	80	85
10	$8.70x10^{-3}$	$4.18x10^{-2}$	$7.13x10^{-2}$	$1.07x10^{-1}$	$1.19x10^{-1}$
100	$5.63x10^{-3}$	$4.30x10^{-2}$	$7.84x10^{-2}$	$1.11x10^{-1}$	$1.30x10^{-1}$
1000	$7.06x10^{-3}$	$4.03x10^{-2}$	$6.94x10^{-2}$	$1.03x10^{-1}$	$1.27x10^{-1}$
10000	$4.36x10^{-3}$	$3.53x10^{-2}$	$7.81x10^{-2}$	$1.06x10^{-1}$	$1.28x10^{-1}$
100000	$5.29x10^{-3}$	$3.47x10^{-2}$	$6.89x10^{-2}$	$1.08x10^{-1}$	$1.21x10^{-1}$
1000000	$6.11x10^{-3}$	$3.43x10^{-2}$	$7.31x10^{-2}$	$1.00x10^{-1}$	$1.29x10^{-1}$
10000[a)]	$6.02x10^{-3}$	$3.58x10^{-2}$	$7.46x10^{-2}$	$1.26x10^{-1}$	$1.24x10^{-1}$

[a)] results of 5000 trial runs.

Table 2: Rate constant(in ps^{-1}) dependency for time step of trajectories using the 6th Symplectic method and the 4th Runge-Kutta method. Other trajectory conditions are as followed: 1000 trial run and total energy is 85 kcal mol^{-1}. Difference between initial total energy and average of total energy by each time step $|< H > -E|$ and variance $< H^2 > - < H >^2$ are also shown.

integrator	time step / fs	k / ps^{-1}	$\|< H > -E\|$	$< H^2 > - < H >^2$
the 6th Symplectic	0.1	0.160	0.000851	0.269
	0.2	0.160	0.00170	0.380
	0.4	0.154	0.00340	0.538
	0.5	0.155	0.00423	0.601
	0.8	0.161	0.00710	0.760
	1.0	0.168	0.0108	0.850
the 4th Runge-Kutta	0.1	0.151	0.000931	0.269
	0.2	0.149	0.00921	0.380
	0.4	0.154	0.146	0.545
	0.5	0.155	0.759	0.708
	0.8	0.147	4.81	2.65
	1.0	0.114	23.2	12.9

Table 3: Microcanonical rate constant $k(E)$ (in cm^{-1}).

	k(E)/ps^{-1}		
E/kcal mol^{-1}	Marks et al.[a)]	constant[b)]	variable[c)]
65	0.019	0.0060	0.0109
66		0.0100	0.0187
67		0.0176	0.0274
68		0.0229	0.0373
69		0.0280	0.0447
70	0.053	0.0358	0.0526
71		0.0435	0.0651
72		0.0523	0.0705
73		0.0568	0.0772
74		0.0619	0.0846
75	0.111	0.0746	0.0891
76		0.0801	0.0962
77		0.0856	0.0994
78		0.0917	0.1118
79		0.1037	0.1101
80	0.171	0.1256	0.1335
81		0.1110	0.1234
82		0.1193	0.1217
83		0.1212	0.1238
84		0.1228	0.1217
85	0.206	0.1241	0.1277

[a)] reference [15]. [b)] this work. $V_{12} = 80$, constant. [c)] this work. $V_{12} = 80 + 50\cos(2\gamma)$.

Table 4: Canonical rate constant $k(T)$ (in s^{-1}).

	$k(T)$			
Temperature / K	Expl.[a)]	Marks et al.[b)]	constant[c)]	variable[d)]
2000	9.753×10^2	5.64×10^3	4.50×10^3	7.62×10^3

[a)] reference [7]. [b)] reference [15]. [c)] this work. $V_{12} = 80$, constant. [d)] this work. $V_{12} = 80 + 50\cos(2\gamma)$.

Table 5: Canonical rate constant $k(T)$ (in s^{-1}) depending parameters A and B at 2000 K.

A[a)]	B[a)]	$k(T)/s^{-1}$	ratio[b)]
80	50	7.62×10^3	1.0
85	50	8.35×10^3	1.09
90	50	8.90×10^3	1.17
95	50	9.61×10^3	1.26
100	50	1.03×10^4	1.35
80	55	8.10×10^3	1.06
80	60	8.48×10^3	1.11
80	65	8.84×10^3	1.16
80	70	9.21×10^3	1.21
80	75	9.63×10^3	1.26

[a)] $V_{12} = A + B\cos(2\gamma)$. [b)] ratio divided by rate constant in the case of A=80 and B=50.

Figure caption

Figure 1. Schematic potential surfaces of N_2O. V_1 and V_2 are the singlet and triplet surfaces, respectively. N-N distance and angle γ are fixed to equilibrium geometry. The definition of γ and R are refered to Figure 2.

Figure 2. N_2O molecule and definition of the Jacobi coordinate.

Figure 3. Distribution of transition point. The horizontal axis is r and the vertical axis is γ, respectively. (a)V_{12}=80 cm^{-1}=constant. (b)V_{12}=80 + 50 cos(γ).

Figure 4. Distribution of transition point. The horizontal axis is R and the vertical axis is γ, respectively. (a)V_{12}=80 cm^{-1}=constant. (b)V_{12}=80 + 50 cos(γ).

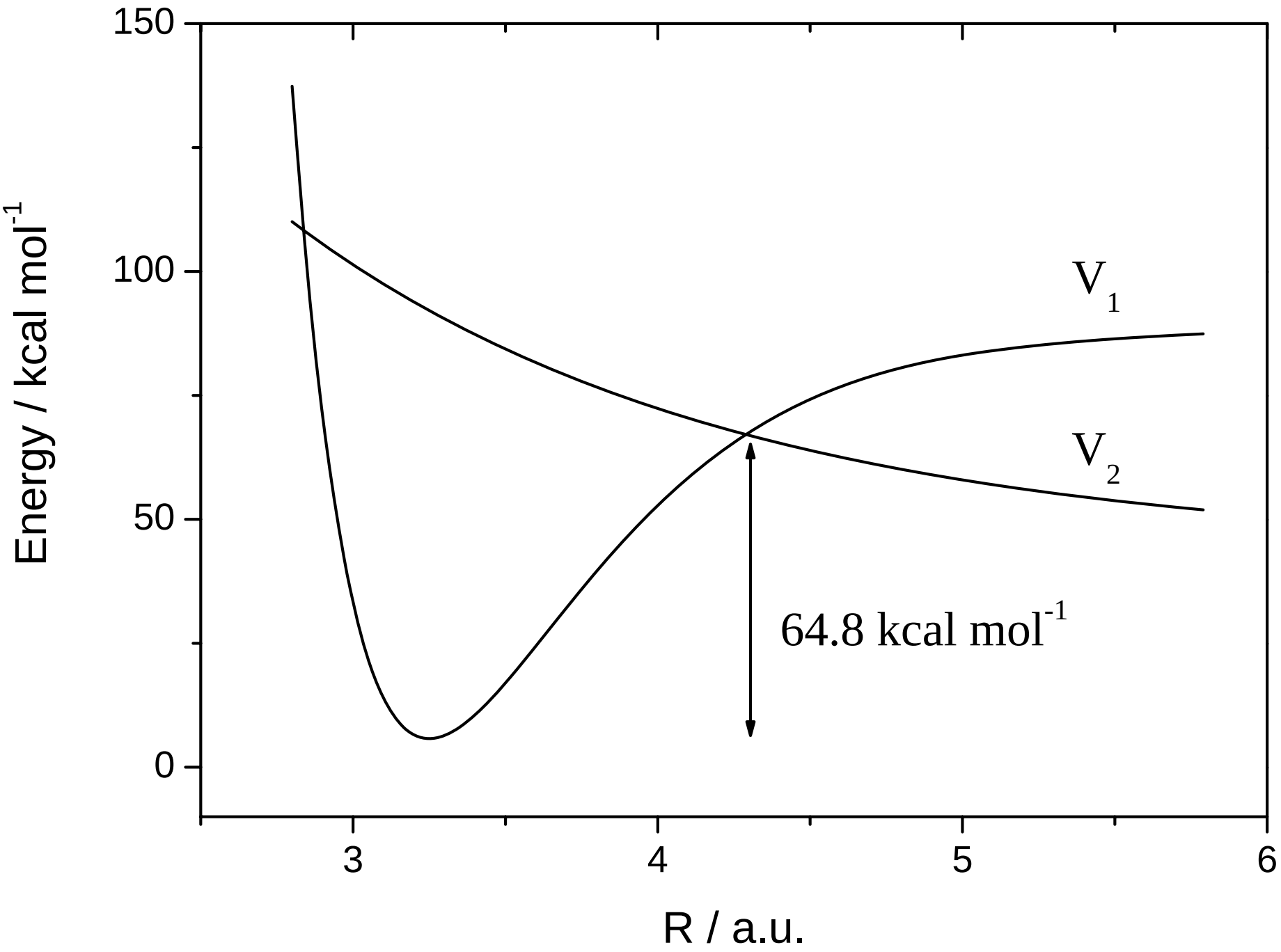

fig.1

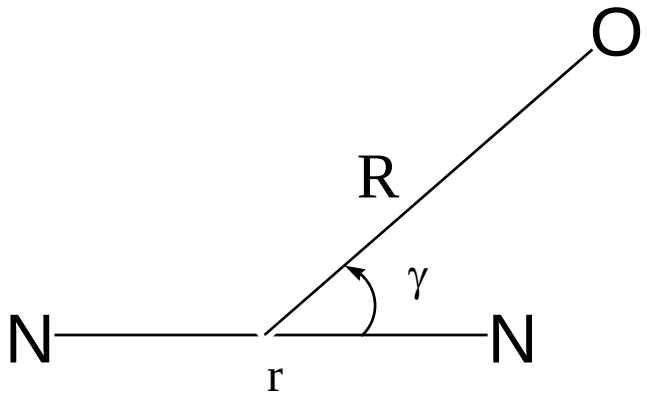

Fig.2

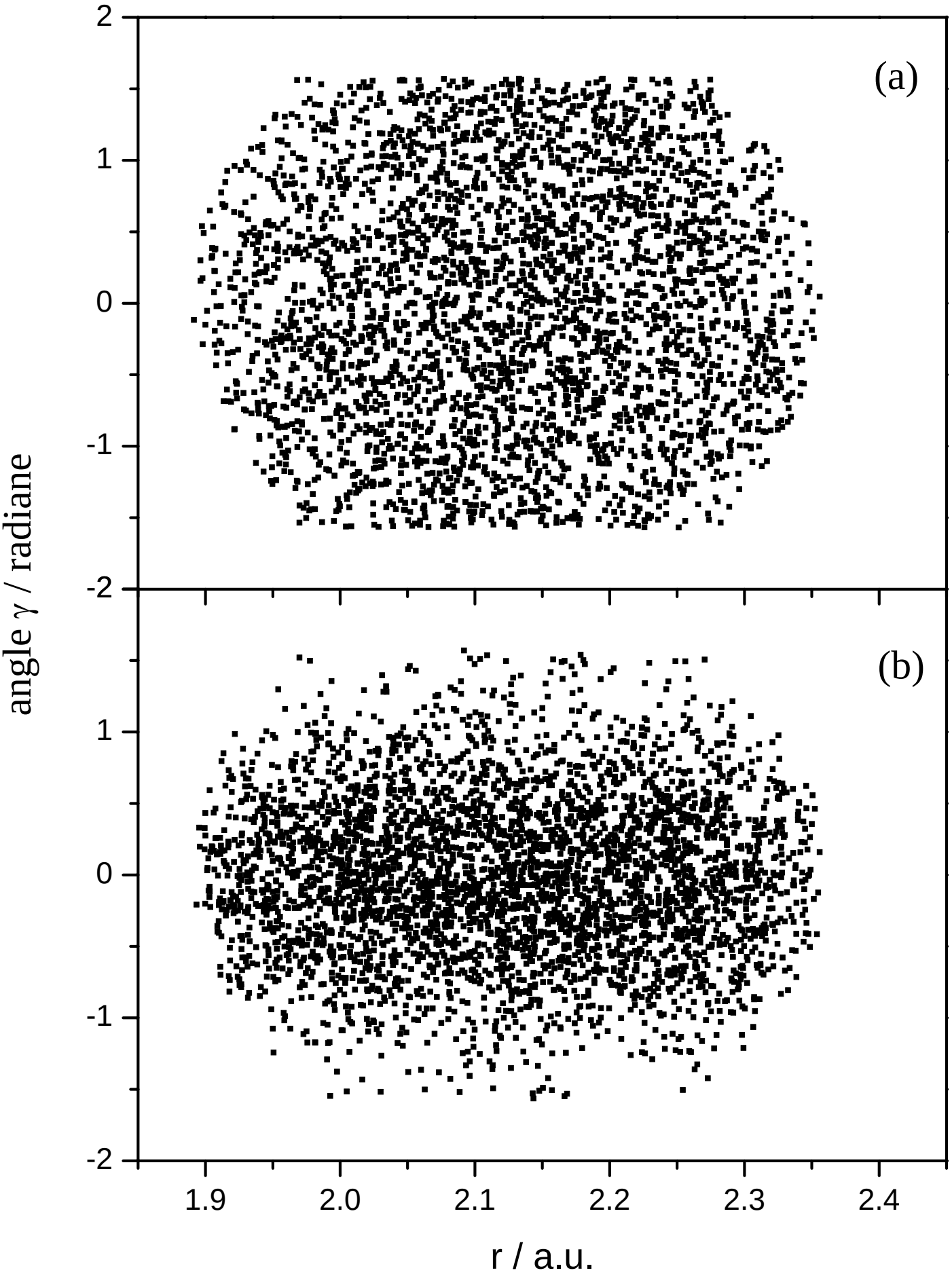

Fig.3

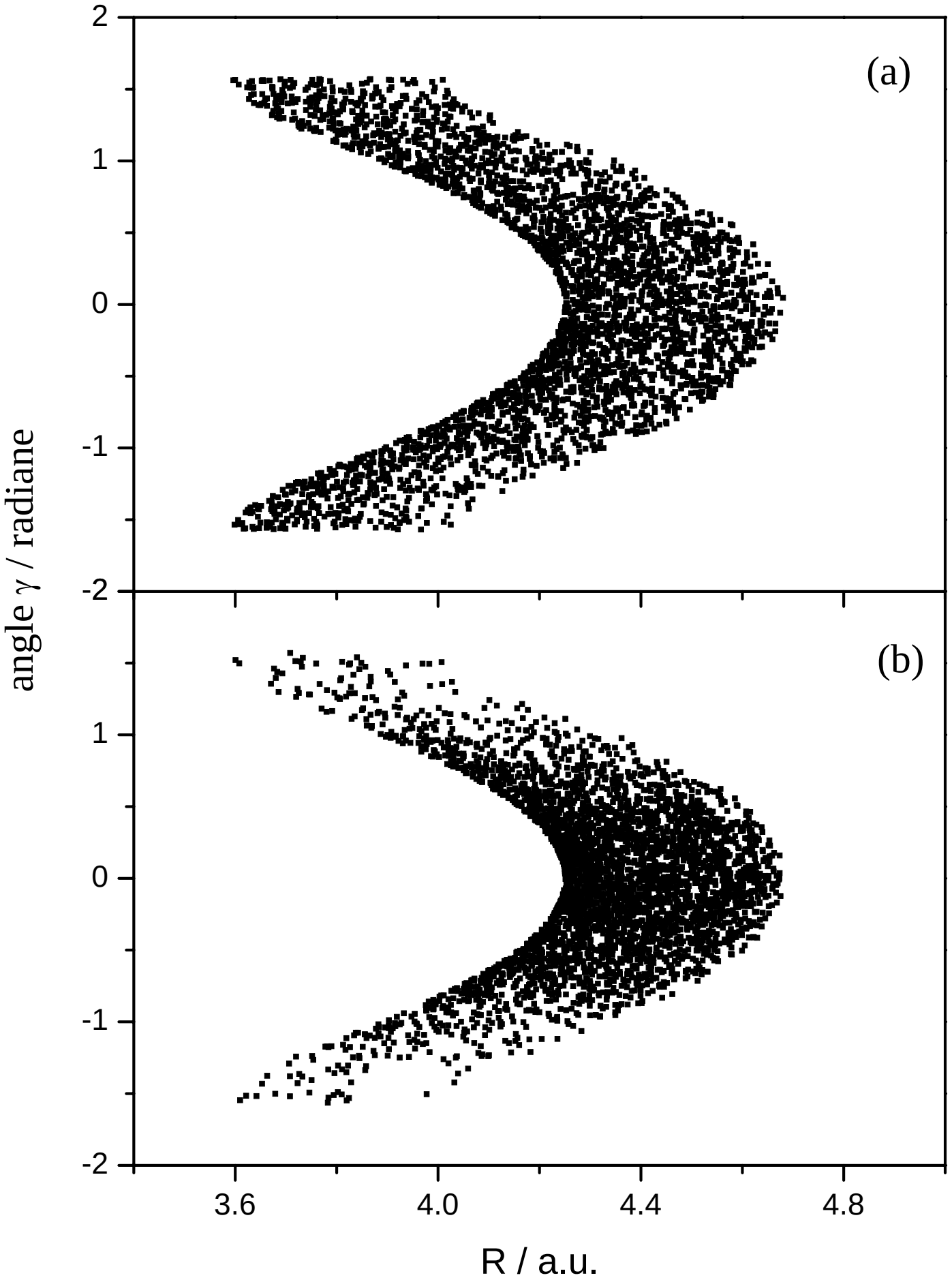

Fig.4